Heliyon 10 (2024) e23426

Contents lists available at ScienceDirect

Heliyon

journal homepage: www.cell.com/heliyon

VDAC1, as a downstream molecule of MLKL, participates in OGD/R-induced necroptosis by inducing mitochondrial damage

Hao Wan [a], Yan-di Yang [a], Qi Zhang [a], Yu-hua Chen [a,b], Xi-min Hu [a], Yan-xia Huang [a], Lei Shang [c,**], Kun Xiong [a,d,e,*]

[a] Department of Anatomy and Neurobiology, School of Basic Medical Science, Central South University, Changsha, China
[b] Department of Central Laboratory, Xi'an Peihua University, Xi'an, China
[c] Jiangxi Research Institute of Ophthalmology and Visual Sciences, Affiliated Eye Hospital of Nanchang University, Nanchang, China
[d] Hunan Key Laboratory of Ophthalmology, Changsha, China
[e] Key Laboratory of Emergency and Trauma, Ministry of Education, College of Emergency and Trauma, Hainan Medical University, Haikou, China

ARTICLE INFO

Keywords:
OGD/R
Necroptosis
MLKL
VDAC1
Mitochondria damage

ABSTRACT

Ischemia-reperfusion (I/R) injury constitutes a significant risk factor for a range of diseases, including ischemic stroke, myocardial infarction, and trauma. Following the restoration of blood flow post-tissue ischemia, oxidative stress can lead to various forms of cell death, including necrosis, apoptosis, autophagy, and necroptosis. Recent evidence has highlighted the crucial role of mitochondrial dysfunction in I/R injury. Nevertheless, there remains much to be explored regarding the molecular signaling network governing cell death under conditions of oxidative stress. Voltage-dependent anion channel 1 (VDAC1), a major component in the outer mitochondrial membrane, is closely involved in the regulation of cell death. In a cellular model of oxygen-glucose deprivation and reoxygenation (OGD/R), which effectively simulates I/R injury *in vitro*, our study reveals that OGD/R induces VDAC1 oligomerization, consequently exacerbating cell death. Furthermore, we have revealed the translocation of mixed lineage kinase domain-like protein (MLKL) to the mitochondria, where it interacts with VDAC1 following OGD/R injury, leading to an increased mitochondrial membrane permeability. Notably, the inhibition of MLKL by necrosulfonamide hinders the binding of MLKL to VDAC1, primarily by affecting the membrane translocation of MLKL, and reduces OGD/R-induced VDAC1 oligomerization. Collectively, our findings provide preliminary evidence of the functional association between MLKL and VDAC1 in the regulation of necroptosis.

1. Introduction

Ischemia/reperfusion (I/R) injury is a prevalent etiology in various clinical diseases. I/R injury occurs as a result of blood flow obstruction to a specific tissue (regional ischemia) and the subsequent reinstatement of blood flow (local perfusion). In severe cases, it can lead to tissue dysfunction [1,2]. Notably, the pathophysiology and pathogenesis of I/R injury are complex [3]. The initial harm in I/R injury arises from tissue hypoxia during ischemia and is further aggravated by tissue damage upon reperfusion [1,2]. During the

* Corresponding author. Department of Anatomy and Neurobiology, School of Basic Medical Science, Central South University, Changsha, China.
** Corresponding author.
E-mail addresses: shanglei1986@ncu.edu.cn (L. Shang), xiongkun2001@163.com (K. Xiong).

https://doi.org/10.1016/j.heliyon.2023.e23426
Received 21 May 2023; Received in revised form 3 December 2023; Accepted 4 December 2023
Available online 11 December 2023

reperfusion phase, inflammatory reactions and oxidative stress can give rise to a cytokine storm, causing damage to cells [4]. Research has revealed that the oxidative stress process can result in mitochondrial damage, and mitochondrial dysfunction has been identified as a central mechanism in I/R injury [3,5,6]. Furthermore, it has been reported that mitochondrial damage can impact necroptosis signals [7,8]. Voltage-dependent anion channel 1 (VDAC1), situated on the outer mitochondrial membrane, plays a pivotal role in controlling the exchange of mitochondrial metabolites and ions with the cytoplasm [9]. VDAC1 is indispensable for the regulation of mitochondrial permeability transition pores (mPTP), which control the opening of mPTP, leading to the leakage of mitochondrial contents such as cytochrome *c* (Cyt *c*), mtDNA [8–12], intracellular Ca^{2+}, and reactive oxygen species (ROS) [13]. Consequently, calcium overload and ROS accumulation can influence cellular function and cell death [9,10,12].

Necroptosis, a form of regulated cell death discovered in recent decades [3,14–20], is characterized by early plasma membrane rupture and organelle swelling, and it has been reported to be a crucial player in I/R injury [21–24]. When necrotic cellular signals are initiated, receptor-interacting serine/threonine kinase 1 (RIPK1) and RIPK3 become activated by death receptors, including tumor necrosis factor receptor 1, toll-like receptor 4 (TLR4), and T cell receptor [21,23]. Subsequently, RIPK3 phosphorylates the necroptotic executioner mixed lineage kinase domain-like protein (MLKL), leading to MLKL oligomerization. MLKL then translocate to the membrane, causing pore formation and the release of intracellular components [16,17,25]. However, the precise mechanism underlying the death signal upon MLKL activation has not been fully elucidated. Recent studies have suggested that MLKL targets not only the plasma membrane but also various other organelle membranes, including lysosomes, mitochondria, endoplasmic reticulum, and nuclei [16,26–28]. MLKL has been reported to activate cell death by translocating to the cell membrane during necroptosis [16,17]. Nevertheless, whether MLKL has functional effects on these organelles remains unclear, and the role of MLKL in mitochondria has not been thoroughly investigated.

In our *in vitro* simulation of I/R injury using oxygen-glucose deprivation and reoxygenation (OGD/R), we present the first evidence that VDAC1 is involved in the regulation of OGD/R-induced necroptosis. We also reveal that MLKL plays a role in regulating mitochondrial damage during OGD/R-induced necroptosis. Furthermore, we explored the potential role of MLKL in necroptosis, and our results reveal that MLKL may be implicated in the regulation of mitochondrial damage after OGD/R injury through its interaction with VDAC1.

2. Materials and methods

2.1. Cell culture and OGD/R treatment

NIH3T3 cells (mouse embryo fibroblast cell line) were kindly gifted by Dr. Jiahuai Han (The Key Laboratory of the Ministry of Education for Cell Biology and Tumor Cell Engineering, School of Life Sciences, Xiamen University, China) and maintained at 37 °C under a 5 % CO_2 atmosphere in high-glucose Dulbecco's modified Eagle's medium (DMEM, Gibco, CA, USA) supplemented with 10 % fetal bovine serum (FBS; Gibco).

OGD/R is commonly used as an *in vitro* model of ischemia [18,19,29–34]. Briefly, the cells were washed with phosphate buffer solution (PBS), the culture medium was replaced with DMEM sugar-free medium (Gibco) and placed in an experimental hypoxia chamber [18,32] composed of 95 % N_2 and 5 % CO_2 (v/v). The cell cultures were exposed to OGD for 3 h. Then, the DMEM sugar-free medium were replaced with fresh high-glucose DMEM (supplemented with 10 % FBS).

2.2. Propidium iodide (PI) staining

PI (10 μg/mL, Sigma, Cat#P4170, Saint Louis, MO, USA) and DAPI (0.5 μg/mL, Beyotime, Cat#C1005, Beijing, China) dual staining were initially performed to determine the necrotic ability of NIH3T3 cells after OGD [18,35]. The blue fluorescence of DAPI represents live and non-viable cells, while the red fluorescence of PI represents necrotic cells. The fluorescent images were photographed using a fluorescence microscope (Olympus, Tokyo, Japan). The PI-positive cells were enumerated with an ImageJ software (NIH, Baltimore, MA, USA).

2.3. siRNA approaches

VDAC1 siRNA, MLKL siRNA, and control siRNA were purchased from RIBO-Biology (China) and used as suggested [18].

The siRNA sequences for *mVdac1* are as follows: (#1): 5′-CCAGAGCAACTTCGCAGTT-3′, (#2): 5′-CCATTTACCAGAAGGTGAA-3′, (#3): 5′-GCTTCGGAATAGCAGCCAA-3′. The transfections were performed with Lipofectamine 3000 (Thermo Scientific, Invitrogen, CA, USA) and Opti-MEM (Gibco) according to the manufacturer's protocol.

The siRNA sequences for *Mlkl* are as follows: (#1): 5′-AUGCAGAGGAAGACGGAAATT-3′, (#2): 5′-CGGAAACACUCCACAGAAATT3′, (#3): 5′-GCACUAAAGCAGAGAGAUCTT-3′. The transfections were performed with Lipofectamine 3000 (Thermo Scientific) and Opti-MEM (Gibco) according to the manufacturer's instructions.

2.4. Drug application

Necrostatin-1 (Nec-1, Selleck, Cat#S8037, China) is a potent necroptosis inhibitor that targets RIPK1 within the necroptosis pathway [24,36]. It was initially dissolved in dimethyl sulfoxide (DMSO, Sigma) to create a stock solution. NIH3T3 cells were pretreated with 20 μM Nec-1 for 2 h to inhibit OGD/R-induced necroptosis. Necrosulfonamide (NSA, Med Chem Express, Cat#HY-100573,

CA, USA) is a necroptosis inhibitor that selectively targets MLKL [37,38]. It was also dissolved in DMSO to create a stock solution. NIH3T3 cells were pretreated with 5 μM NSA for 4 h before inducing the OGD/R model to inhibit necroptosis. VBIT-12 (Selleck, Cat#S8936) is a potent inhibitor of VDAC1, directly interacting with VDAC1 and interfering with its oligomerization [11,39]. It was also dissolved in DMSO as a stock solution. NIH3T3 cells were pretreated with 25 μM VBIT-12 for 4 h prior to implementing the OGD/R model to inhibit necroptosis. The final concentration of DMSO did not exceed 0.1 %.

2.5. Lactate dehydrogenase (LDH) release assay

To measure the release of LDH from necrotic cells into the extracellular space/supernatant following the different treatments, we employed the LDH cytotoxicity assay kit (Beyotime, Cat#C0016) [18,35]. The intensity of the red color produced in the assay was measured via absorbance at a wavelength of 490 nm using a 96-well microplate reader (Bio-rad, CA, USA). The observed value was proportional to LDH activity and the percentage of necrotic cells.

2.6. Western blot (WB) analysis

Proteins were extracted from cell lysates using radioimmunoprecipitation (CWBIO, China) buffer containing a protease inhibitor cocktail (CWBIO). The concentrations of soluble proteins in the lysate were determined using a BCA protein assay kit (CWBIO, Cat#CW0014). Equal amounts of proteins were separated using 10 % sodium dodecyl sulfate (SDS)-polyacrylamide gel before being transferred to polyvinylidene fluoride membranes (Millipore, Billerica, MA, USA). The proteins of interest on the membranes were incubated with corresponding primary antibodies, IgG-HRP (1:5,000, Jackson Immuno Research, USA), and visualized by exposing them to enhanced chemiluminescence WB reagents. The Tanon™ 5200CE Chemi-Image System (Tanon, Shanghai, China) was used to scan the chemiluminescent blots. Finally, the density of the bands was quantified using ImageJ software (Syngene, Frederick, MD, USA). The primary antibodies used included anti-VDAC1 (1:1,000, Abcam, Cat#ab154856, USA), anti-MLKL (1:1,000, Proteintech, Cat#66675, China), anti-phospho-MLKL (1:1,000, Cell Signaling Technology, Cat#37333, USA), anti-GAPDH (1:2,000, Affinity Biosciences, Cat#AF7021, China), and anti-β-actin (1:2,000, Affinity Biosciences, Cat#AF7018).

2.7. Co-immunoprecipitation (Co-IP)

Cell lysis was performed using Pierce IP Lysis Buffer (Thermo Fisher Scientific) according to the instructions. Antibodies (rabbit anti-MLKL antibody, Proteintech, Cat#66675, China; rabbit anti-MLKL (phospho S345) antibody, Abcam, Cat# ab196436; rabbit anti-VDAC1 antibody, Abcam, Cat#ab247271; rabbit anti-IgG, Beyotime, Cat#A7016) were added to lysates with protein A + G Agarose (Santa Cruz Biotechnology, Inc., CA, USA) and incubated overnight at 4 °C.

Following centrifugation, the deposit was collected and washed with dilution/wash buffer (10 mM Tris-HCl, pH 7.5, 150 mM NaCl, 0.5 mM EDTA) three times. After resuspension in the SDS sample buffer, it was boiled for 5 min. The boiled compounds were re-centrifuged, and the supernatant was used for subsequent WB.

2.8. Mitochondrial sample preparation

Mitochondrial-enriched fractions were prepared using a mitochondrial extraction kit (Solarbio, Cat# SM0020, China) as per the manufacturer's protocol. The mitochondrial-enriched pellet was reconstituted in a storage buffer after collection and was processed for WB analysis.

2.9. Measurement of intracellular calcium ion

Intracellular Ca^{2+} levels were evaluated using the fluorescent Ca^{2+} indicator fluo-3-acetoxymethylester AM (Fluo-3 AM, Beyotime, Cat#S1056) [40,41]. Fluorescent images were captured using a fluorescence microscope (Olympus). Single-cell calcium quantification was performed using a Cyflow Space flow cytometer, and the cell percentages were analyzed using FlowJo software (FlowJo LLC, USA).

The intracellular calcium concentration was determined with a Calcium Colorimetric Assay kit (Beyotime, Cat#S1063S). Briefly, the collected cells were lysed with a lysate buffer and incubated with the appropriate reagent mixture following the manufacturer's instructions at room temperature for 10 min. Finally, the absorbance at 575 nm was measured using a 96-well microplate reader (Bio-Rad).

2.10. Measurement of mitochondrial membrane potential (MMP)

MMP was quantified using the fluorescent JC-1 assay kit (Beyotime, Cat#C2006). After OGD/R injury, cells were washed twice with a buffer solution and incubated in a culture medium supplemented with JC-1 for 20 min at 37 °C in the dark. Subsequently, the cells were washed twice with buffer solution, and fluorescent images were captured using a fluorescence microscope (Olympus).

2.11. Measurement of ROS intensity

To measure ROS, the 2'-7' dichlorofluorescin diacetate (DCFH-DA) probe (Beyotime, Cat#S0033S) was used. Cells were gently washed two times with serum-free medium after OGD/R injury, and 10 μm of DCFH-DA was added to each well, followed by incubation at 37 °C in the dark for 30 min. The cells were then washed with serum-free medium three times to remove uninternalized DCFH-DA. Fluorescent images were captured using a fluorescence microscope (Olympus).

2.12. Chemical crosslinking

To detect VDAC1 oligomerization, ethylene glycol bis(succinimidyl succinate) (EGS) (GLPBIO), a chemical crosslinking agent, was used [42]. After OGD/R injury, cells were trypsinized, centrifuged at 1500×*g* for 5 min, washed once with PBS, and incubated with 0.5 mM EGS at room temperature for 30 min. Crosslinking was halted with 10 mM Tris-HCl (pH 7.8) and incubated for an additional 15 min at room temperature. Samples were subsequently collected after centrifugation at 1500×*g* for 5 min.

2.13. Statistics analyses

Statistical analyses were conducted using GraphPad Prism software, and data were presented as mean ± standard deviation. A two-way analysis of variance was performed to assess inter-group differences, and Dunnett or Tukey post-hoc tests were conducted for comparisons. Statistical significance was established at $p < 0.05$.

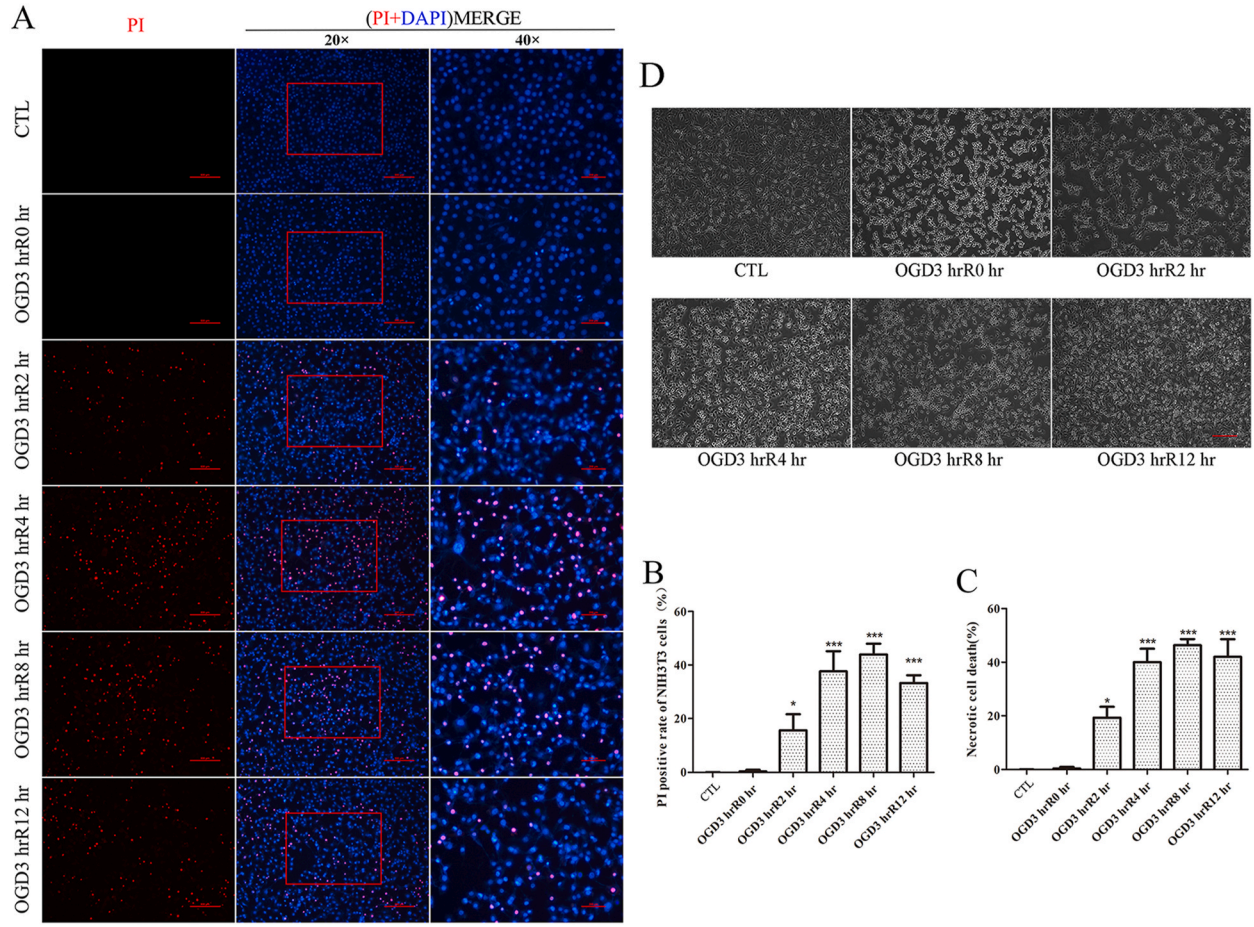

Fig. 1. Necrosis was determined by PI staining and LDH release assay after OGD injury. (A) PI staining of NIH3T3 after OGD/R injury. PI positive (red) represents necrotic cells, the nucleus were counterstained with DAPI (blue). Scale bars: 500 μm (all images on the left and middle column); 200 μm (all panels on the right column). (B) The statistical analysis of PI/DAPI staining of necrotic cells. *$p < 0.05$ *vs.* CTL group; ***$p < 0.001$ *vs.* CTL group. (C) The percentage of NIH3T3 necrosis was determined by LDH release assay. *$p < 0.05$ *vs.* CTL group; ***$p < 0.001$ *vs.* CTL group. (D) Microscopic visualization of cell morphology after OGD/R injury. Scale bars: 200 μm.

3. Results

3.1. OGD/R injury-induced necroptosis

Necrotic cell death, as indicated by changes in cell membrane permeability, was assessed through PI staining and LDH release assays. As observed through PI and DAPI counterstaining, NIH3T3 cells exhibited time-dependent damage following OGD for 3 h and then various recovery periods (0 h, 2 h, 4 h, 8 h, and 12 h), respectively (Fig. 1A). Quantitative analysis revealed a significant increase in necrotic cell death at 2 h, 4 h, 8 h, and 12 h after recovery from OGD/R injury compared to the CTL group (Fig. 1B). The LDH release assay results mirrored the PI staining findings, with the percentage of necrotic cells being significantly higher in the OGD/R group at 2 h, 4 h, 8 h, and 12 h after recovery, in comparison to the CTL and 0 h groups (Fig. 1C). Changes in cell morphology were observed under brightfield microscopy, and significant alterations in cell morphology were noted following OGD/R injury (Fig. 1D). These results collectively indicate that OGD/R injury induced necrosis in NIH3T3 cells, with cellular necrosis occurring approximately 2–12 h after OGD/R injury. Similar outcomes were observed when R28 cells were subjected to OGD/R, which also led to the necrosis of R28 cells (Supplementary Fig. 1).

Pretreatment of cells with the potent necroptosis inhibitors Nec-1 and NSA, followed by OGD/R injury, resulted in noteworthy findings. PI and DAPI counterstaining revealed a lack of PI-positive cells in the CTL group. However, the OGD/R injury group exhibited a significant increase in PI-positive cells. Notably, pretreatment with Nec-1 or NSA reduced OGD/R-induced injury and necrosis compared to the control OGD/R group (Fig. 2A and B and Supplementary Fig. 2 A, 2B). The LDH release assay findings were in

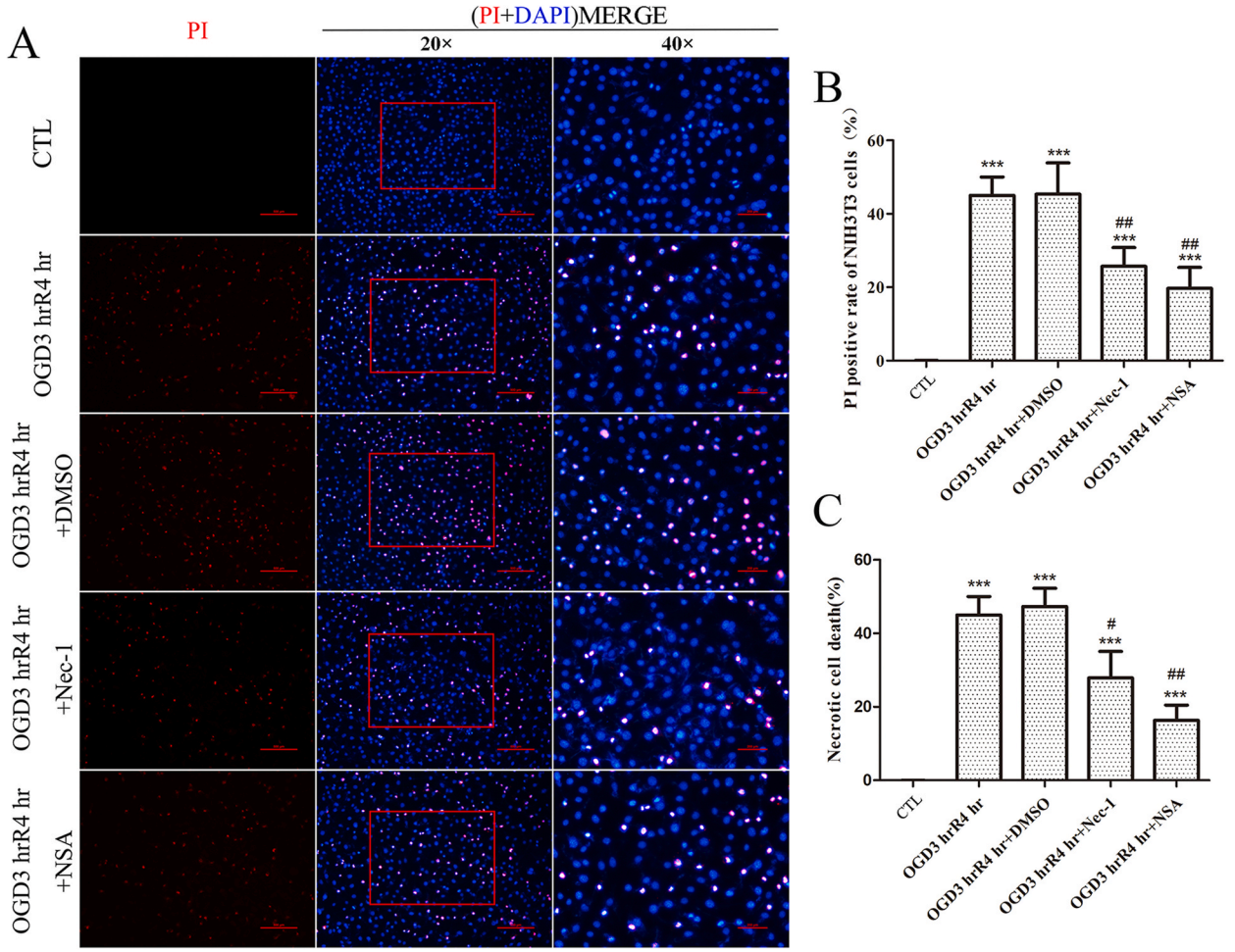

Fig. 2. Necroptotic cell death was determined by PI staining and LDH release assay *via* Nec-1 and NSA pretreatment following OGD injury. (A) PI staining detects OGD injury-induced necrosis of NIH3T3 after Nec-1 and NSA pretreatment. PI positive (red) represents necrotic cells, the nucleus were counterstained with DAPI (blue). Scale bars: 500 μm (all images on the left and middle column); 200 μm (all panels on the right column). (B) The statistical analysis of PI/DAPI staining of necrotic cells. $^{**}p < 0.001$ *vs.* CTL group; $\#\#p < 0.01$ *vs.*OGD3 hr R 4 h group. (C) The percentage of NIH3T3 necrosis was determined by LDH release assay. $^{***}p < 0.001$ *vs.* CTL group; $\#p < 0.05$ *vs.* OGD3 hr R 4 h group; $\#\#p < 0.01$ *vs.* OGD3 hr R 4 h group.

agreement with the PI staining results, with LDH release significantly increased in the OGD/R group compared to the CTL group. Furthermore, the necrosis observed in the groups pretreated with Nec-1 or NSA was significantly reduced compared to the OGD/R group (Fig. 2C and Supplementary Fig. 2 C), indicating that Nec-1 and NSA effectively inhibited OGD/R-induced necrosis in NIH3T3 cells. Altogether, these results highlight the occurrence of necroptosis following OGD/R injury in NIH3T3 cells and R28 cells.

3.2. Upregulation of VDAC1 expression and MLKL phosphorylation in OGD/R injury

Based on our previous findings where I/R injury led to the activation of MLKL and alterations in intracellular Ca^{2+} [18,19,32], we hypothesized that MLKL might play a role in the changes in intracellular Ca^{2+} levels following OGD/R injury. To investigate the functions of MLKL and VDAC1 in OGD/R injury, we initially assessed the alterations in MLKL protein levels, phosphorylation, and VDAC1 levels using WB analysis (Fig. 3A and Supplementary Fig. 3A). Quantification and statistical analysis of the WB results revealed a significant increase in both MLKL and VDAC1 protein levels after OGD/R in comparison to the CTL group (Fig. 3B and Supplementary Fig. 3B). Importantly, MLKL phosphorylation significantly increased at 4 h, 8 h, and 12 h after recovery from OGD injury in NIH3T3 cells (Fig. 3A and B) and MLKL phosphorylation significantly increased at 2 h, 4 h, and 8 h after recovery from OGD injury in R28 cells

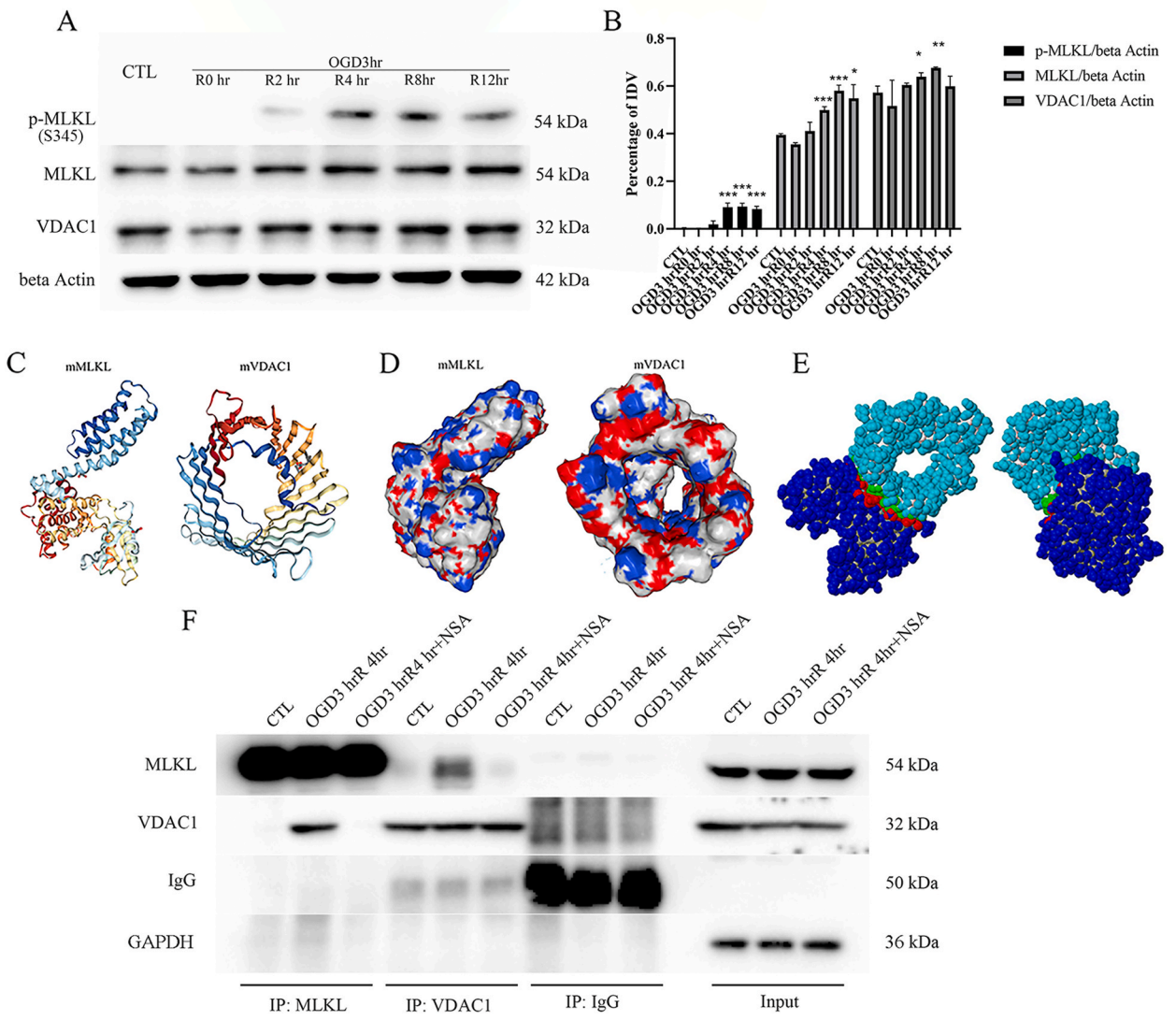

Fig. 3. The expression of MLKL and VDAC1 following OGD treatment and interaction between MLKL and VDAC1. (A) The protein expression level of *p*-MLKL, MLKL, and VDAC1 in NIH3T3 following OGD was determined by Western blot. (B) The statistical analysis of protein expression level of *p*-MLKL, MLKL, and VDAC1 in NIH3T3 after OGD treatment. $*p < 0.05$ *vs.* CTL group; $**p < 0.01$ *vs.* CTL group; $***p < 0.001$ *vs.* CTL group. (C) The spatial protein structure of MLKL and VDAC1. (D) The protein surface electrostatic potential energy diagram of MLKL and VDAC1 (negative densities are shown in red, and positive peaks are shown in green). (E) A software simulation diagram of the interaction between MLKL and VDAC1 by zDOCK. (F) Co-IP assay of MLKL and VDAC1 in NIH3T3.

(Supplementary Fig. 3). Subsequently, we acquired structural models of MLKL and VDAC1 from the Protein Data Bank (http://www.rcsb.org/pdb/) and employed software to simulate a hypothetical complex of these two molecules (Fig. 3C). Protein surface potential analysis was conducted using ChimeraX software (NIH, Baltimore, MD, USA) [43] (Fig. 3D). We further employed the zDock Server for Interactive Docking Prediction of MLKL and VDAC1 [44], where the scoring functions incorporated three terms: IFACE statistical potential, shape complementarity, and electrostatics (Fig. 3E). These results indicated a potential interaction between MLKL and VDAC1. To validate the molecular docking results, Co-IP was used. WB analysis revealed the binding of MLKL and VDAC1 to each other after OGD/R injury, with NSA-pretreated cells inhibiting this interaction (Fig. 3F). Therefore, these findings collectively support the

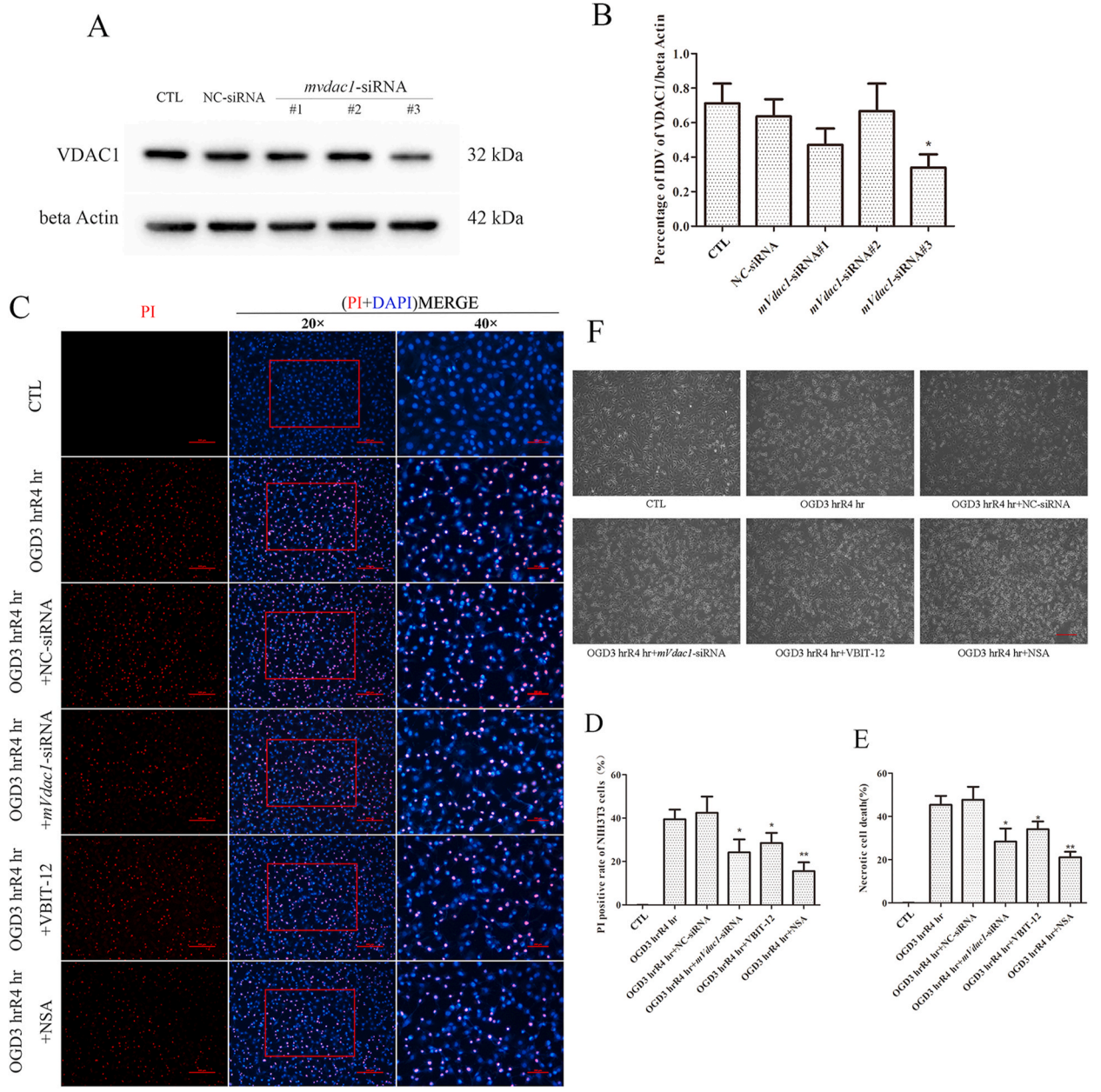

Fig. 4. MLKL and VDAC1 participate in regulating necroptosis following OGD/R injury. (A) VDAC1 protein expression level after *mVdac1*-siRNA intervention. (B) Statistical analysis of the changes in the protein expression level of VDAC1, $*p < 0.05$ *vs.* CTL group. (C) PI staining of NIH3T3 after different treatments. PI positive (red) represents necrotic cells, the nucleus were counterstained with DAPI (blue). Scale bars: 500 μm (all images on the left and middle column); 200 μm (all panels on the right column). (D) The statistical analysis of PI/DAPI staining of necrotic cells. $*p < 0.05$ *vs.* OGD 3 h R 4 h group; $**p < 0.01$ *vs.* OGD3 hr R 4 h group. (E) The percentage of NIH3T3 necrosis was determined by LDH release assay. $*p < 0.05$ *vs.* OGD3 hr R 4 h group; $**p < 0.01$ *vs.* OGD3 hr R 4 h group. (F) Microscopic visualization of cell morphology after OGD/R injury. Scale bars: 200 μm.

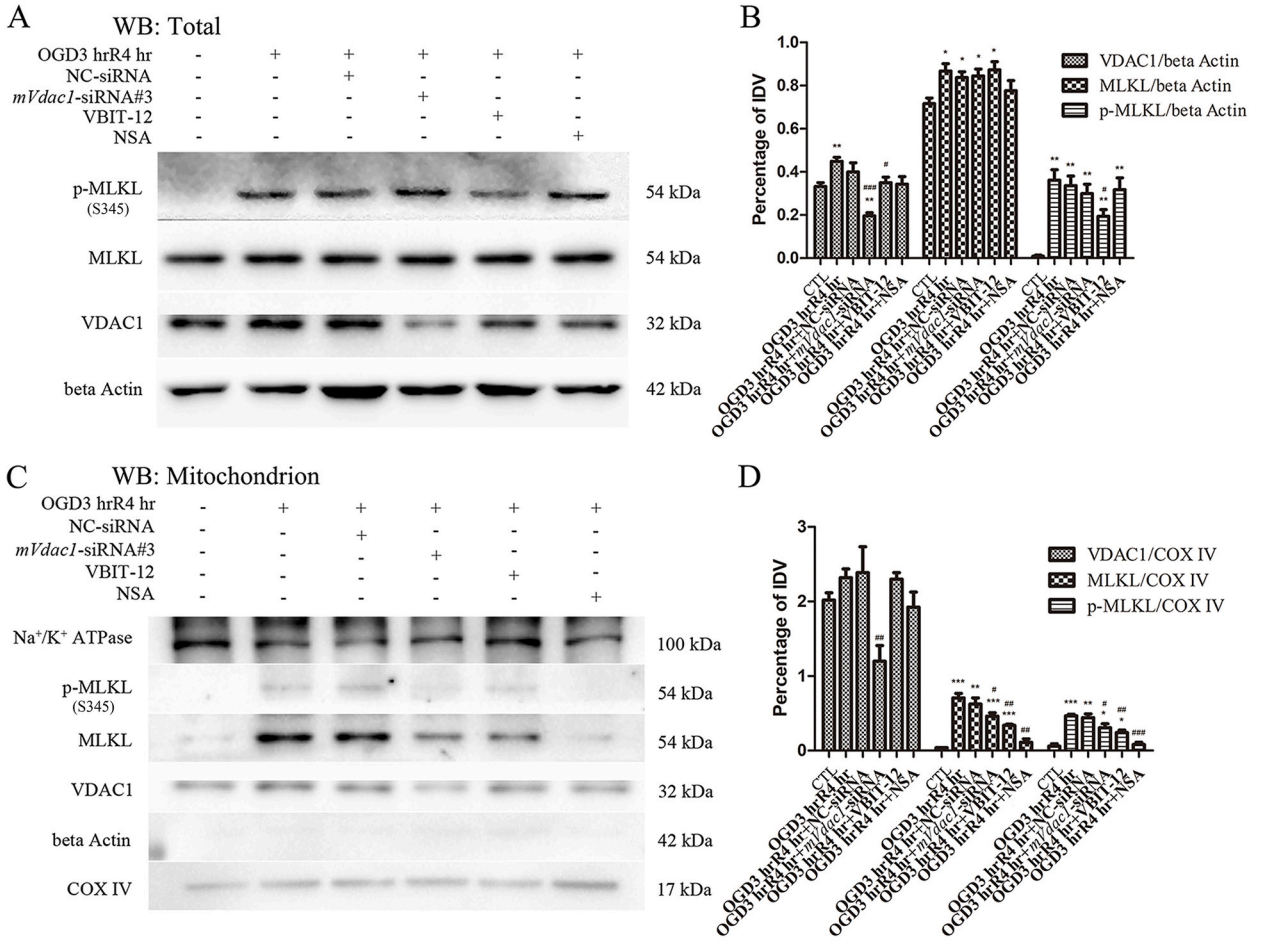

(caption on next page)

Fig. 5. VDAC1 participates in MLKL membrane localization. (A) Changes in the protein expression level of *p*-MLKL, MLKL, and VDAC1 in whole cell extraction after OGD injury by Western blot. (B) Statistical analysis of protein expression of *p*-MLKL, MLKL, and VDAC1 after OGD injury in total protein. $*p < 0.05$ *vs.* CTL group; $**p < 0.01$ *vs.* CTL group; $\#p < 0.05$ *vs.* OGD3 hr R 4 h group; $\#\#\#p < 0.001$ *vs.* OGD3 hr R 4 h group. (C) Changes in the protein expression level of *p*-MLKL, MLKL, and VDAC1 in mitochondrial extraction after OGD injury by Western blot. (D) Statistical analysis of protein expression level of *p*-MLKL, MLKL, VDAC1 after OGD injury in mitochondrial protein. $*p < 0.05$ *vs.* CTL group; $**p < 0.01$ *vs.* CTL group; $***p < 0.001$ *vs.* CTL group; $\#p < 0.05$ *vs.* OGD3 hr R 4 h group; $\#\#p < 0.01$ *vs.* OGD3 hr R 4 h group; $\#\#\#p < 0.001$ *vs.* OGD3 hr R 4 h group. (E) Transfect MLKL S345A or MLKL S345D in $MLKL^{-/-}$ NIH3T3 cells and label mitochondria with pDsRed2-mito. Capture fluorescence images after OGD/R injury by Fluorescence microscopy. Scale bars: 20 μm.

hypothesis that MLKL and VDAC1 may bind together during OGD/R injury.

3.3. Knocking down or inhibiting VDAC1 protein expression reduced OGD/R-induced necroptosis in NIH3T3 cells

To investigate the role of VDAC1 in necroptosis, we designed an siRNA to interfere with VDAC1 protein expression, followed by evaluation by performing WB. Following siRNA transfection in NIH3T3 cells, VDAC1 protein expression decreased significantly after treatment with *mVdac1*-siRNA#3, indicating the optimal effect of *mVdac1*-siRNA#3 (Fig. 4A and B). Thus, *mVdac1*-siRNA#3 was selected for subsequent experiments, and hereafter, *mVdac1*-siRNA is specifically referred to as *mVdac1*-siRNA#3. Additionally, we pretreated NIH3T3 cells or R28 cells with VBIT-12, an inhibitor of VDAC1 that inhibits VDAC1 oligomerization, to inhibit VDAC1 activity before OGD/R injury. The results showed that in the *mVdac1*-siRNA and VBIT-12 pretreatment groups, the number of PI-positive cells was significantly lower than that in the CTL group (Fig. 4C and Supplementary Fig. 4A). The statistical analysis showed that pretreatment with *mVdac1-si*RNA and VBIT-12 led to a significant reduction in OGD/R injury-induced cell death (Fig. 4D and Supplementary Fig. 4B). Furthermore, the LDH release assay results were similar to those of PI staining, in which the levels of cell death after pretreatment with *mVdac1*-siRNA and VBIT-12 decreased significantly compared with that in the OGD/R group (Fig. 4E and Supplementary Fig. 4C). Moreover, the microscopic observation of cell morphology showed that pretreatment with m*Vdac1*-siRNA, VBIT-12, or NSA significantly alleviated the OGD/R-induced changes in cell morphology (Fig. 4F). These results suggest that VDAC1 plays a crucial role in OGD/R-induced necroptosis in NIH3T3 cells; thus, VDAC1 activity or expression inhibition can reduce OGD/R-induced necroptosis.

3.4. VDAC1 affects MLKL translocation

To evaluate the effect of VDAC1 on MLKL translocation to the mitochondria, we extracted whole-cell and mitochondrial proteins to detect their expression by WB (Fig. 5A). In the case of whole-cell proteins, MLKL expression levels were not significantly altered in the NSA, *mVdac1*-siRNA, or VBIT-12 pretreatment groups compared with those in the OGD/R group. Conversely, *p*-MLKL expression bands in the VBIT-12 pretreatment group decreased compared with those in the OGD/R group. Additionally, VDAC1 expression bands were weak in the *mVdac1*-siRNA and VBIT-12 pretreatment groups compared with those in the OGD/R group (Fig. 5B). In the case of mitochondrial proteins, a few positive bands of MLKL and *p*-MLKL were detected in the CTL group. In comparison, significant MLKL and *p*-MLKL bands were detected in the OGD/R and NC-siRNA treatment groups. Pretreatment with NSA, *mVdac1*-siRNA, or VBIT-12 significantly reduced the positive bands of mitochondrial MLKL and *p*-MLKL in the OGD/R group (Fig. 5C and D). These results showed that VDAC1 interfered with MLKL localization in the mitochondrial membrane or suppressed MLKL function, indicating the important role of VDAC1 in MLKL translocation.

RIPK3 can activate the MLKL via S345 phosphorylation, thereby causing a conformational change of MLKL that enables its translocation to the plasma membrane [17,25–28].

To validate the molecular docking results, Co-IP was used. WB analysis revealed the binding of *p*-MLKL (phospho S345) and VDAC1 to each other after OGD/R injury, with NSA-pretreated cells inhibiting this interaction (Fig. 3F). Therefore, these findings collectively support the hypothesis that MLKL and VDAC1 may bind together during OGD/R injury. We perform Co-IP with *p*-MLKL (phospho S345) antibody, WB analysis revealed the binding of *p*-MLKL (phospho S345) and VDAC1 to each other after OGD/R injury, with NSA-pretreated cells inhibiting this interaction (Supplementary Fig. 5). To investigate whether the phosphorylation of MLKL were involved in MLKL mitochondrial localization, we reconstituted MLKL mutants, a mutant of MLKL S345D (Phosphorylation mimics mutations at S345 site), or MLKL S345A (that cannot be phosphorylated at S345), and labeled mitochondria with pDsRed2-mito. The results showed that MLKL S345D, MLKL S345A and pDsRed2-mito were uniformly distributed in the cytoplasm in normal condition, and after OGD/R treatment, MLKL S345D showed more co-localization with red-labeled mitochondria than that of MLKL S345A in NIH3T3 cells (Fig. 5E). This suggests that oligomerization and *trans*-location of MLKL S345D to mitochondria may occur after OGD/R injury, indicating that MLKL mitochondrial localization associates with phosphorylation of the S345 site.

3.5. MLKL plays a role in changes in intracellular Ca^{2+} concentrations by affecting VDAC1 functions

Mitochondria is one of the main sites for intracellular Ca^{2+} concentration regulation [5,9,45]. Herein, we determined the relationship between the roles of MLKL and VDAC1 and the corresponding changes in intracellular Ca^{2+} concentrations. Fluo-3 AM was used to detect intracellular Ca^{2+} concentrations (Fig. 6A). The fluorescence intensity of the OGD/R group increased significantly compared with that of the CTL group. The fluorescence intensity was attenuated in the *mVdac1*-siRNA, VBIT-12, and NSA pretreatment groups compared with that in the OGD/R group, and the number of cells with high Ca^{2+} concentration increased significantly in the

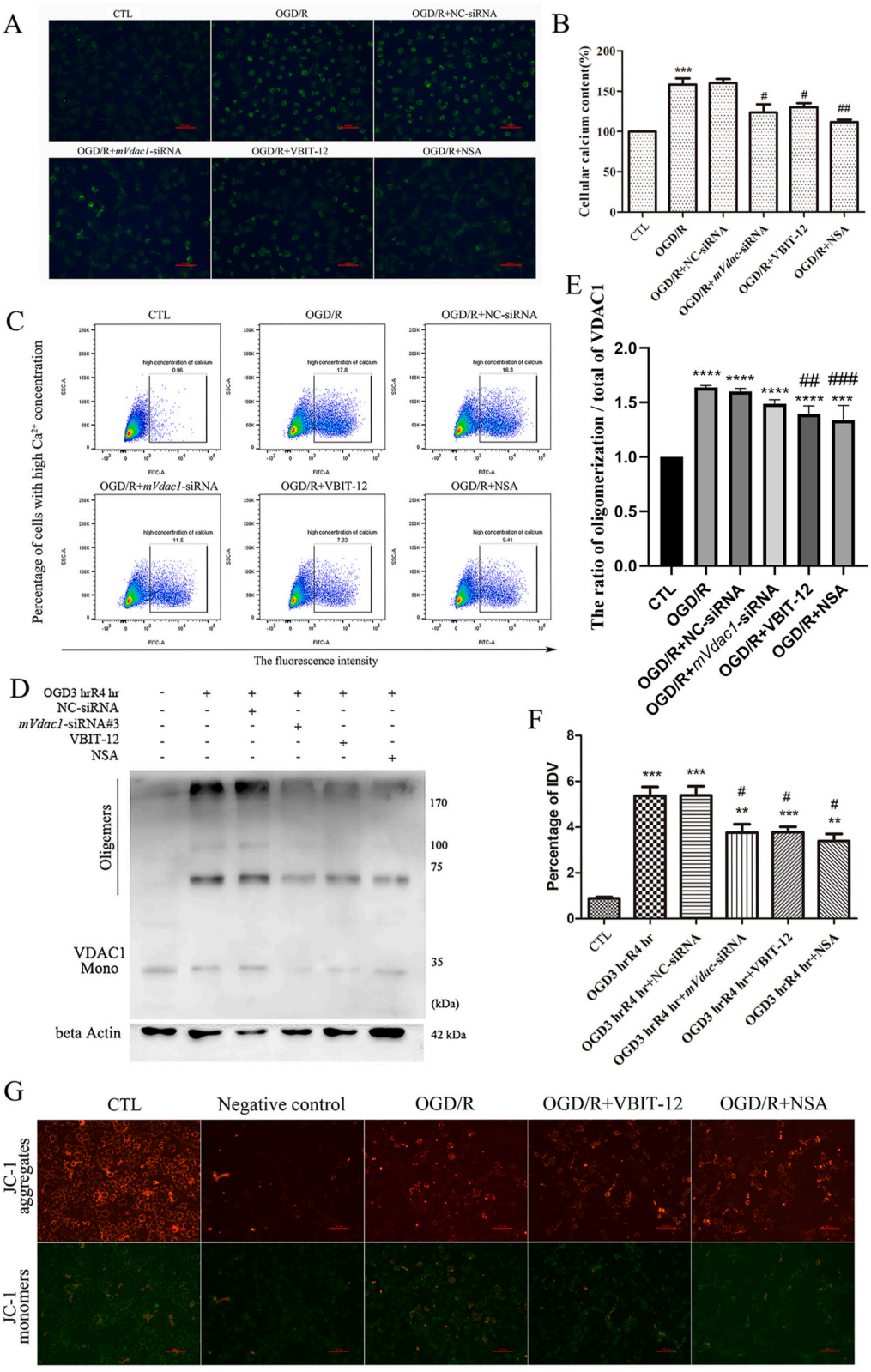

(caption on next page)

Fig. 6. MLKL is involved in OGD-induced mitochondrial damage processes through the oligomerization of VDAC1. (A) Fluo-3 AM tag was used to detect the changes in the concentration of calcium ions in NIH3T3 cells after OGD injury, and Fluo-3 AM combined with calcium ions emits green fluorescence; Scale bars: 200 μm. (B) The intracellular concentration of the calcium ion detection kit was used to assess changes in intracellular calcium ion concentrations in NIH3T3 cells after OGD injury. ***$p < 0.001$ *vs.* CTL group; #$p < 0.05$ *vs.* OGD3 hr R 4 h group; ##$p < 0.01$ *vs*. OGD3 hr R 4 h group. (C) Calcium ion fluorescence intensity was detected by flow cytometry after Fluo-3 AM treatment. (D) Changes in the VDAC1 oligomerization form in whole cell extraction treated with EGS (ethylene glycol bis (succinimidyl succinate)) after OGD injury. (E) Statistical analysis of the ratio of oligomerization VDAC1 to total VDAC1. ***$p < 0.001$ *vs.* CTL group; ****$p < 0.001$ *vs.* CTL group; ##$p < 0.01$ *vs.* OGD3 hr R 4 h group; ###$p < 0.001$ *vs.* OGD3 hr R 4 h group. (F) Statistical analysis of the VDAC1 oligomerization/beta Actin in total cell extraction treated with EGS after OGD injury. **$p < 0.01$ *vs.* CTL group; ***$p < 0.001$ *vs.* CTL group; #$p < 0.05$ *vs.* OGD3 hr R 4 h group. (G) JC-1 was used to detect mitochondrial dysfunction, CTL mitochondrial membrane potential (red), and depolarized membrane potentials (green).

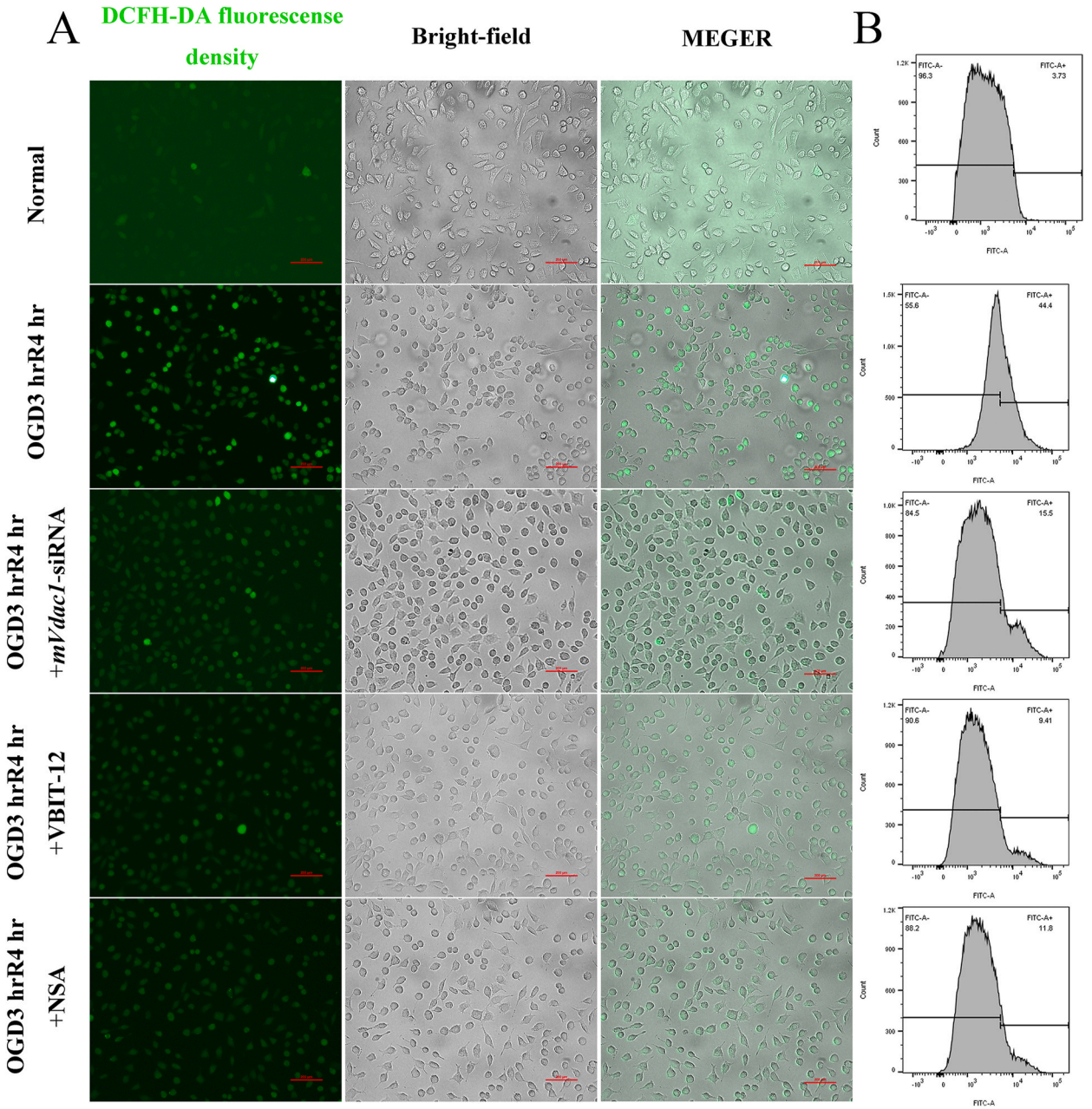

Fig. 7. MLKL and VDAC1 are involved in the OGD-induced ROS generation. (A) Changes in the concentration of intracellular ROS after OGD injury, and the DCFH-DA probe combined with ROS emits green fluorescence, which was observed by fluorescence microscopy (All groups were treated with DCFH-DA) ; Scale bars: 200 μm. (B) ROS fluorescence intensity was detected by flow cytometry after DCFH-DA treatment.

OGD/R group compared with that in the CTL, *mVdac1*-siRNA, and VBIT-12 groups (Fig. 6C). Pretreatment with NSA reduced this increase owing to OGD/R damage. Next, intracellular Ca^{2+} concentrations were quantified using a Ca^{2+} concentration detection kit, and the results were similar to the fluorescence results, showing that the intracellular Ca^{2+} concentration increased significantly compared with that in the CTL group. Furthermore, Ca^{2+} concentrations were lower in the *mVdac1*-siRNA, VBIT-12, and NSA groups than in the OGD/R group owing to pretreatment with *mVdac1*-siRNA, VBIT-12, and NSA after OGD/R injury (Fig. 6B). Therefore, these results suggest that inhibiting the functions of MLKL and VDAC1 may prevent the increase in intracellular Ca^{2+} concentrations after OGD/R injury. Combined with previous results, these results indicate that MLKL plays a role in changes in Ca^{2+} concentrations by regulating VDAC1 function during necroptosis.

3.6. MLKL plays a role in mitochondrial damage by regulating VDAC1 oligomerization in OGD/R-induced necroptosis

The above results suggested that VDAC1 oligomerization during OGD/R injury might contribute to mitochondrial dysfunction and that VDAC1 interacted with MLKL. Thus, we examined the function of MLKL in mitochondrial dysfunction. We designed siRNAs to interfere with the expression of MLKL. Following siRNA transfection in NIH3T3 cells, MLKL expression significantly decreased after treatment with *mMlkl*-siRNA#1 (Supplementary Figs. 6A and 6B). Thus, *mMlkl*-siRNA#1 was selected for subsequent experiments, and hereafter, *mMlkl*-siRNA is specifically referred to as *mMlkl*-siRNA#1. We treated the cell-extracted proteins by EGS and then detected VDAC1 bands by performing WB. The results showed fewer VDAC1 oligomerization bands in the CTL group. Conversely, VDAC1 oligomerization bands significantly increased after OGD/R injury (Supplementary Fig. 7), and *mVdac1-si*RNA, *mMlkl*-siRNA, VBIT-12, or NSA pretreatment significantly reduced this increase(Fig. 6D, E, F, and Supplementary Figs. 6 and 8). These results showed OGD/R injury-induced VDAC1 oligomerization, indicating that MLKL might be involved in VDAC1 oligomerization. Furthermore, we performed JC-1 staining to identify the depolarization of mitochondrial membrane potential, which is an indicator of mitochondrial damage. The results showed that the number of cells with CTL mitochondrial membrane potential in the OGD/R group decreased significantly compared with that in the CTL group. Conversely, after pretreatment with NSA or VBIT-12, the number of cells with CTL mitochondrial membrane potential increased compared with that in the OGD/R group (Fig. 6G). Simultaneously, we performed ROS staining and found that intracellular fluorescence intensity in the OGD/R group was higher than that in the CTL group. Compared with the OGD/R group, the NSA, VBIT-12, or *mVdac1*-siRNA pretreatment groups showed significantly decreased intracellular fluorescence intensity (Fig. 7 and Supplementary Fig. 9). These results suggested that OGD/R injury induced intracellular ROS production, which led to mitochondrial damage. The above findings indicate that MLKL plays a role in OGD/R-induced mitochondrial damage by regulating VDAC1 oligomerization.

4. Discussion

I/R injury may trigger various biochemical and molecular mechanisms, thereby leading to the loss of mitochondrial membrane potential or oxidative damage and resulting in altered intracellular ion concentrations [46], energy depletion, and cell death [1,47,48]. Necroptosis, a RIPK1-, RIPK3-, and MLKL-dependent regulated cell death phenomenon [16,17,25,27,28], is characterized by the permeabilization of the plasma membrane and the release of disease-associated molecular patterns (DAMPs) [26,49]. The release of DAMPs may induce immune responses and inflammation. Further, necroptosis plays an important role in I/R injury [3,50,51]. Studies have found weakened I/R injury of the kidneys of RIPK3-deficient mice [52], as well as some studies have shown that RIPK3 deficiency reduces cardiac hypertrophy and inflammation after myocardial infarction [53]. Moreover, the inhibition of RIPK3 and MLKL expression can reduce cell death induced by I/R injury, thereby exerting a protective effect by suppressing oxidative stress, necrosis, and inflammation [54–56]. Thus, necroptosis may be the mainstay of acute ischemic injury. Elucidating the underlying mechanism of necroptosis will help develop new therapeutic targets and effective strategies for treating I/R injury.

We previously found that MLKL phosphorylation occurred in OGD/R (a classic model for simulating I/R injury *in vitro*), which induced necrosis [18,19,32], indicating that MLKL played a vital role in necroptosis. Additionally, MLKL phosphorylation and translocation during OGD/R induced necroptosis in NIH3T3 cells. Two studies showed MLKL translocation and identified MLKL as a prominent molecule related to necroptosis [26,27]. MLKL translocation to the cell membrane can trigger the rupture of the cell membrane and eventually lead to cell death [26–28]. Subsequent studies have shown MLKL translocation to organelles including the mitochondria and nucleus [16,28,57]; however, the biological role of these cellular events is unclear. Herein, we investigated new regulatory mechanisms of programmed necrosis-related pathways in I/R injury and provided new ideas for treating programmed necrosis I/R-related diseases.

Cellular Ca^{2+} overload is an important factor in necrosis [14,15]. Notably, the *in vivo* regulation of Ca^{2+} is complicated. I/R injury can lead to mitochondrial damage, resulting in increased intracellular Ca^{2+} and ROS production, thereby triggering subsequent signals and ultimately leading to cell damage [4,5]. Additionally, CaMKII plays an essential role in necroptosis, and the RIPK3-mediated phosphorylation of CaMKII promotes the opening of the mPTP channel; thus, it can be involved in Ca^{2+} regulation during necroptosis; RIPK3 deficiency or CaMKII inhibition can ameliorate Ca^{2+} overload induced by I/R [58]. However, we found that OGD/R increased intracellular Ca^{2+} concentration. Furthermore, NSA, a functional inhibitor of MLKL, suppressed the increase in intracellular Ca^{2+} concentration during OGD/R-induced cell death. Therefore, we thought that MLKL might be involved in the increase in Ca^{2+} concentration induced by I/R injury. Considering that MLKL acts as one of the classical targeting molecules for RIPK3, we speculated that RIPK3 knockdown alleviated I/R-induced Ca^{2+} overload in the previous study by decreasing MLKL phosphorylation levels following RIPK3 knockout.

Many factors control changes in intracellular Ca^{2+} concentrations [45,59,60]. Herein, we found that MLKL inhibitors attenuated

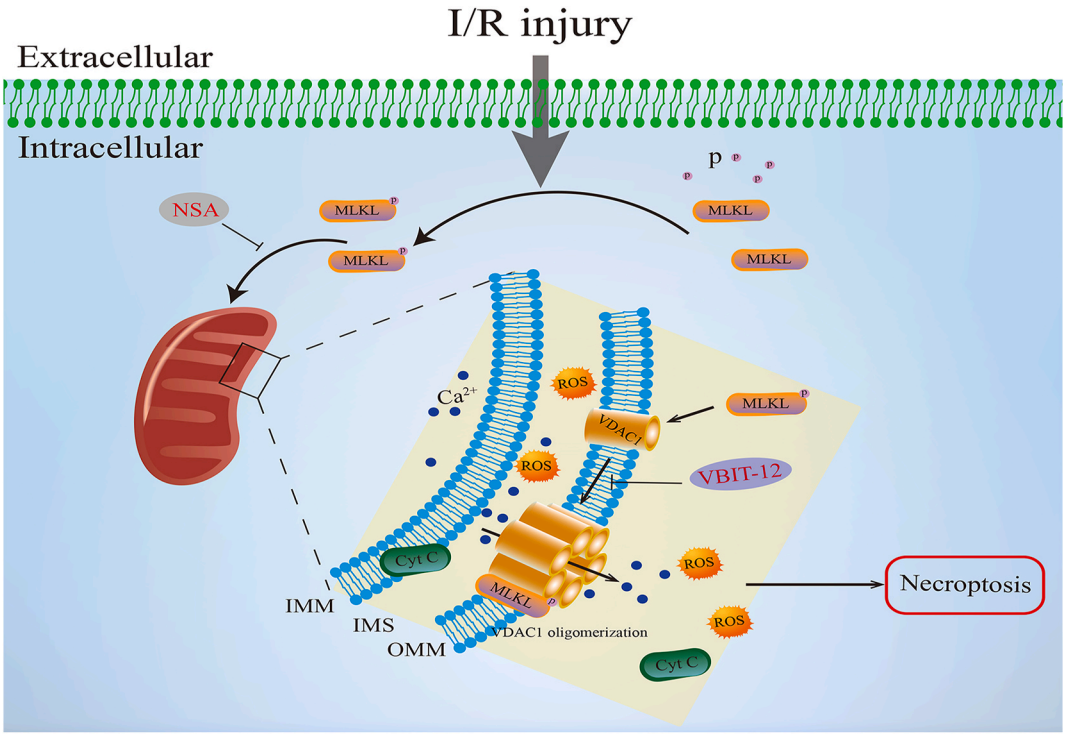

Fig. 8. VDAC1 as a downstream molecule of MLKL to regulate mitochondrial damage during necroptosis. IMM: Inner mitochondrial membrane; IMS: Inner mitochondrial space; OMM: Outer mitochondrial membrane.

OGD/R-induced mitochondrial damage, which is one of the leading causes of the intracellular Ca^{2+} concentration imbalance [7,8,12,61]. Therefore, we associated the effect of MLKL on intracellular Ca^{2+} concentration changes with mitochondrial damage for a better understanding of I/R injury-related diseases in order to develop new treatment strategies.

Accumulating evidence has shown the disruption of mitochondrial permeability during necroptosis [7,10,11,61,62], and the transduction of necrosis signals can disrupt mitochondrial homeostasis [7,8]. Mitochondrial homeostasis imbalance can reduce ATP synthesis and induce ROS accumulation [45,48,50]. Furthermore, ROS can trigger RIPK phosphorylation and lead to necroptosis [61,63,64]. We found that OGD/R induced mitochondrial mPTP channel opening and NSA inhibited OGD/R-induced mitochondrial damage and ROS release. Therefore, we hypothesized that MLKL might be associated with OGD/R-induced mitochondrial damage.

VDAC1 plays a vital role in the alteration of mitochondrial outer membrane permeability [9–13]. One hypothesis is that VDAC1 oligomerization is involved in the continuous opening of mPTP channels, which leads to cell death [62,65]. Moreover, the present WB results showed that VDAC1 expression increased after OGD/R injury. To investigate the regulatory mechanism of MLKL during mitochondrial damage, we isolated mitochondrial proteins interacting with MLKL after OGD/R by performing Co-IP assays and identified them by performing mass spectrometry (our unpublished data). In our study, we found that VDAC1 probably interacted with MLKL. As mentioned, VDAC1 participated in mPTP channel opening by undergoing oligomerization to regulate mitochondrial damage. Additionally, VDAC1 oligomerization increased significantly after OGD/R, whereas NSA inhibited this process and reduced OGD/R-induced mitochondrial damage, ultimately reducing necroptosis. Therefore, we speculate that MLKL may regulate mitochondrial damage by affecting VDAC1 oligomerization to regulate necroptosis. However, the specific interaction of VDAC1 with MLKL should be further investigated in the future.

In conclusion, the present results preliminarily show that MLKL can localize to mitochondria after OGD/R injury, and MLKL possesses the potential to participate in mitochondrial damage by regulating VDAC1 oligomerization during OGD/R-induced necroptosis (Fig. 8). Notably, these findings indicate a potential target for OGD/R injury-related diseases, and suggest VDAC1 as a valuable target in treating I/R-related diseases.

Data availability

All the data used to support the findings of this study are included within the article and the supplementary materials. Additional data related to this paper may be requested from the authors.

CRediT authorship contribution statement

Hao Wan: Writing - review & editing, Writing - original draft, Data curation, Conceptualization. **Yan-di Yang:** Data curation. **Qi Zhang:** Writing - review & editing, Supervision, Funding acquisition, Conceptualization. **Yu-hua Chen:** Writing - review & editing, Data curation. **Xi-min Hu:** Writing - review & editing, Data curation. **Yan-xia Huang:** Writing - review & editing, Data curation. **Lei Shang:** Writing - review & editing, Supervision, Resources, Conceptualization. **Kun Xiong:** Writing - review & editing, Supervision, Funding acquisition, Conceptualization.

Declaration of competing interest

The authors declare that they have no known competing financial interests or personal relationships that could have appeared to influence the work reported in this paper.

Acknowledgments

This work was supported by National Natural Science Foundation of China (grant numbers 81971891, 82072229, 81900861, 82172196 and 82372507), Jiangxi Provincial Natural Science Foundation (grant numbers 20202BABL206061), Hunan Provincial Natural Science Foundation (grant numbers 2023JJ40804), Key Laboratory of Emergency and Trauma (Hainan Medical University) of Ministry of Education (grant numbers KLET-202210), Research Foundation of Jiangxi Provincial Commission of Health (grant numbers 202210718), Postgraduate Research and Innovation Project of Hunan Province (grant numbers CX20220322), Innovation Project for Graduate Students at Central South University (grant numbers 2021zzts0312), and College Students' Innovation and Entrepreneurship Project (grant numbers S20210026020013).

Appendix A. Supplementary data

Supplementary data to this article can be found online at https://doi.org/10.1016/j.heliyon.2023.e23426.

References

[1] M.Y. Wu, G.T. Yiang, W.T. Liao, A.P. Tsai, Y.L. Cheng, P.W. Cheng, et al., Current Mechanistic concepts in ischemia and reperfusion injury, Cell. Physiol. Biochem. 46 (4) (2018) 1650–1667.
[2] B. Dorweiler, D. Pruefer, T.B. Andrasi, S.M. Maksan, W. Schmiedt, A. Neufang, et al., Ischemia-reperfusion injury : pathophysiology and clinical implications, Eur. J. Trauma Emerg. Surg. 33 (6) (2007) 600–612.
[3] C.C. Hsu, C.C. Huang, L.H. Chien, M.T. Lin, C.P. Chang, H.J. Lin, et al., Ischemia/reperfusion injured intestinal epithelial cells cause cortical neuron death by releasing exosomal microRNAs associated with apoptosis, necroptosis, and pyroptosis, Sci Rep-Uk 10 (1) (2020).
[4] L. Wu, X. Xiong, X. Wu, Y. Ye, Z. Jian, Z. Zhi, et al., Targeting oxidative stress and inflammation to prevent ischemia-reperfusion injury, Front. Mol. Neurosci. 13 (2020) 28.
[5] F. Liu, J. Lu, A. Manaenko, J. Tang, Q. Hu, Mitochondria in ischemic stroke: new Insight and implications, Aging Dis 9 (5) (2018) 924–937.
[6] Y.D. Yang, Z.X. Li, X.M. Hu, H. Wan, Q. Zhang, R. Xiao, et al., Insight into crosstalk between Mitophagy and apoptosis/necroptosis: mechanisms and clinical Applications in ischemic stroke, Curr Med Sci 42 (2) (2022) 237–248.
[7] J. Wang, H. Zhou, Mitochondrial quality control mechanisms as molecular targets in cardiac ischemia-reperfusion injury, Acta Pharm. Sin. B 10 (10) (2020) 1866–1879.
[8] C. Xue, X. Gu, G. Li, Z. Bao, L. Li, Mitochondrial mechanisms of necroptosis in liver diseases, Int. J. Mol. Sci. 22 (1) (2020).
[9] V. Shoshan-Barmatz, Y. Krelin, A. Shteinfer-Kuzmine, VDAC1 functions in Ca(2+) homeostasis and cell life and death in health and disease, Cell Calcium 69 (2018) 81–100.
[10] V. Shoshan-Barmatz, E. Nahon-Crystal, A. Shteinfer-Kuzmine, R. Gupta, VDAC1, mitochondrial dysfunction, and Alzheimer's disease, Pharmacol. Res. 131 (2018) 87–101.
[11] A. Verma, S. Pittala, B. Alhozeel, A. Shteinfer-Kuzmine, E. Ohana, R. Gupta, et al., The role of the mitochondrial protein VDAC1 in inflammatory bowel disease: a potential therapeutic target, Mol. Ther. 30 (2) (2022) 726–744.
[12] V. Shoshan-Barmatz, A. Shteinfer-Kuzmine, A. Verma, VDAC1 at the Intersection of cell metabolism, apoptosis, and diseases, Biomolecules 10 (11) (2020).
[13] S. Feno, G. Butera, D. Vecellio Reane, R. Rizzuto, A. Raffaello, Crosstalk between calcium and ROS in Pathophysiological conditions, Oxid. Med. Cell. Longev. 2019 (2019), 9324018.
[14] P. Zhu, S. Hu, Q. Jin, D. Li, F. Tian, S. Toan, et al., Ripk3 promotes ER stress-induced necroptosis in cardiac IR injury: a mechanism involving calcium overload/XO/ROS/mPTP pathway, Redox Biol. 16 (2018) 157–168.
[15] M. Barati, M.A. Javidi, B. Darvishi, S.P. Shariatpanahi, Z.S. Mesbah Moosavi, R. Ghadirian, et al., Necroptosis triggered by ROS accumulation and Ca(2+) overload, partly explains the inflammatory responses and anti-cancer effects associated with 1Hz, 100 mT ELF-MF in vivo, Free Radic. Biol. Med. 169 (2021) 84–98.
[16] A.L. Samson, Y. Zhang, N.D. Geoghegan, X.J. Gavin, K.A. Davies, M.J. Mlodzianoski, et al., MLKL trafficking and accumulation at the plasma membrane control the kinetics and threshold for necroptosis, Nat. Commun. 11 (1) (2020) 3151.
[17] J. Zhao, S. Jitkaew, Z. Cai, S. Choksi, Q. Li, J. Luo, et al., Mixed lineage kinase domain-like is a key receptor interacting protein 3 downstream component of TNF-induced necrosis, Proc. Natl. Acad. Sci. U. S. A. 109 (14) (2012) 5322–5327.
[18] M. Wang, H. Wan, S. Wang, L. Liao, Y. Huang, L. Guo, et al., RSK3 mediates necroptosis by regulating phosphorylation of RIP3 in rat retinal ganglion cells, J. Anat. 237 (1) (2020) 29–47.
[19] W.T. Yan, W.J. Zhao, X.M. Hu, X.X. Ban, W.Y. Ning, H. Wan, et al., PANoptosis-like cell death in ischemia/reperfusion injury of retinal neurons, Neural Regen Res 18 (2) (2023) 357–363.
[20] W.T. Yan, Y.D. Yang, X.M. Hu, W.Y. Ning, L.S. Liao, S. Lu, et al., Do pyroptosis, apoptosis, and necroptosis (PANoptosis) exist in cerebral ischemia? Evidence from cell and rodent studies, Neural Regen Res 17 (8) (2022) 1761–1768.

[21] A. Linkermann, J.H. Brasen, M. Darding, M.K. Jin, A.B. Sanz, J.O. Heller, et al., Two independent pathways of regulated necrosis mediate ischemia-reperfusion injury, Proc. Natl. Acad. Sci. U. S. A. 110 (29) (2013) 12024–12029.
[22] J. Li, J. Zhang, Y. Zhang, Z. Wang, Y. Song, S. Wei, et al., TRAF2 protects against cerebral ischemia-induced brain injury by suppressing necroptosis, Cell Death Dis. 10 (5) (2019) 328.
[23] M. Lu, X.X. Fang, D.D. Shi, R. Liu, Y. Ding, Q.F. Zhang, et al., A selective TRPC3 inhibitor Pyr3 Attenuates myocardial ischemia/reperfusion injury in mice, Curr Med Sci 40 (6) (2020) 1107–1113.
[24] B. Shen, M. Mei, Y. Pu, H. Zhang, H. Liu, M. Tang, et al., Necrostatin-1 Attenuates Renal ischemia and reperfusion injury via Meditation of HIF-1alpha/mir-26a/TRPC6/PARP1 signaling, Mol. Ther. Nucleic Acids 17 (2019) 701–713.
[25] L. Sun, H. Wang, Z. Wang, S. He, S. Chen, D. Liao, et al., Mixed lineage kinase domain-like protein mediates necrosis signaling downstream of RIP3 kinase, Cell 148 (1–2) (2012) 213–227.
[26] X. Chen, W. Li, J. Ren, D. Huang, W.T. He, Y. Song, et al., Translocation of mixed lineage kinase domain-like protein to plasma membrane leads to necrotic cell death, Cell Res. 24 (1) (2014) 105–121.
[27] Z. Cai, S. Jitkaew, J. Zhao, H.C. Chiang, S. Choksi, J. Liu, et al., Plasma membrane translocation of trimerized MLKL protein is required for TNF-induced necroptosis, Nat. Cell Biol. 16 (1) (2014) 55–65.
[28] H. Wang, L. Sun, L. Su, J. Rizo, L. Liu, L.F. Wang, et al., Mixed lineage kinase domain-like protein MLKL causes necrotic membrane disruption upon phosphorylation by RIP3, Mol Cell 54 (1) (2014) 133–146.
[29] Y.Y. Wang, C.Y. Chang, S.Y. Lin, J.D. Wang, C.C. Wu, W.Y. Chen, et al., Quercetin protects against cerebral ischemia/reperfusion and oxygen glucose deprivation/reoxygenation neurotoxicity, J. Nutr. Biochem. 83 (2020), 108436.
[30] B. Mathew, S. Ravindran, X. Liu, L. Torres, M. Chennakesavalu, C.C. Huang, et al., Mesenchymal stem cell-derived extracellular vesicles and retinal ischemia-reperfusion, Biomaterials 197 (2019) 146–160.
[31] M.G. Ryou, R.T. Mallet, An in vitro oxygen-glucose deprivation model for studying ischemia-reperfusion injury of Neuronal cells, Methods Mol. Biol. 1717 (2018) 229–235.
[32] L. Liao, L. Shang, N. Li, S. Wang, M. Wang, Y. Huang, et al., Mixed lineage kinase domain-like protein induces RGC-5 necroptosis following elevated hydrostatic pressure, Acta Biochim. Biophys. Sin. 49 (10) (2017) 879–889.
[33] H. Wan, Y.D. Yan, X.M. Hu, L. Shang, Y.H. Chen, Y.X. Huang, et al., Inhibition of mitochondrial VDAC1 oligomerization alleviates apoptosis and necroptosis of retinal neurons following OGD/R injury, Ann. Anat. 247 (2023), 152049.
[34] Z. Zhou, L. Shang, Q. Zhang, X. Hu, J.F. Huang, K. Xiong, DTX3L induced NLRP3 ubiquitination inhibit R28 cell pyroptosis in OGD/R injury, Biochim. Biophys. Acta Mol. Cell Res. 1870 (3) (2023), 119433.
[35] A.E. Kabakov, V.L. Gabai, Cell death and Survival assays, Methods Mol. Biol. 1709 (2018) 107–127.
[36] L. Cao, W. Mu, Necrostatin-1 and necroptosis inhibition: pathophysiology and therapeutic implications, Pharmacol. Res. 163 (2021), 105297.
[37] L. Jing, F. Song, Z. Liu, J. Li, B. Wu, Z. Fu, et al., MLKL-PITPalpha signaling-mediated necroptosis contributes to cisplatin-triggered cell death in lung cancer A549 cells, Cancer Lett. 414 (2018) 136–146.
[38] M. Rubbelke, D. Fiegen, M. Bauer, F. Binder, J. Hamilton, J. King, et al., Locking mixed-lineage kinase domain-like protein in its auto-inhibited state prevents necroptosis, Proc. Natl. Acad. Sci. U. S. A. 117 (52) (2020) 33272–33281.
[39] A. Shteinfer-Kuzmine, S. Argueti-Ostrovsky, M.F. Leyton-Jaimes, U. Anand, S. Abu-Hamad, R. Zalk, et al., Targeting the mitochondrial protein VDAC1 as a potential therapeutic Strategy in ALS, Int. J. Mol. Sci. 23 (17) (2022).
[40] L. Oldach, Democratizing calcium visualization, J. Biol. Chem. 297 (4) (2021), 101181.
[41] S. Zhang, C. Li, J. Gao, X. Qiu, Z. Cui, [Application of the Ca2+ indicator fluo-3 and fluo-4 in the process of H2O2 induced apoptosis of A549 cell], Zhongguo Fei Ai Za Zhi 17 (3) (2014) 197–202.
[42] Z. Gao, Q. Shang, Z. Liu, C. Deng, C. Guo, Mitochondrial ATF2 translocation contributes to apoptosis induction and BRAF inhibitor resistance in melanoma through the interaction of Bim with VDAC1, Oncotarget 6 (34) (2015) 36338–36353.
[43] E.F. Pettersen, T.D. Goddard, C.C. Huang, E.C. Meng, G.S. Couch, T.I. Croll, et al., UCSF ChimeraX: structure visualization for researchers, educators, and developers, Protein Sci. 30 (1) (2021) 70–82.
[44] B.G. Pierce, K. Wiehe, H. Hwang, B.H. Kim, T. Vreven, Z. Weng, ZDOCK server: interactive docking prediction of protein-protein complexes and symmetric multimers, Bioinformatics 30 (12) (2014) 1771–1773.
[45] I.B. Zavodnik, [Mitochondria, calcium homeostasis and calcium signaling], Biomed. Khim. 62 (3) (2016) 311–317.
[46] E. Besancon, S. Guo, J. Lok, M. Tymianski, E.H. Lo, Beyond NMDA and AMPA glutamate receptors: emerging mechanisms for ionic imbalance and cell death in stroke, Trends Pharmacol. Sci. 29 (5) (2008) 268–275.
[47] S. Cadenas, ROS and redox signaling in myocardial ischemia-reperfusion injury and cardioprotection, Free Radic. Biol. Med. 117 (2018) 76–89.
[48] S. Di Meo, T.T. Reed, P. Venditti, V.M. Victor, Harmful and Beneficial role of ROS, Oxid. Med. Cell. Longev. 2016 (2016), 7909186.
[49] Y.S. Cho, S. Challa, D. Moquin, R. Genga, T.D. Ray, M. Guildford, et al., Phosphorylation-driven assembly of the RIP1-RIP3 complex regulates programmed necrosis and virus-induced inflammation, Cell 137 (6) (2009) 1112–1123.
[50] Y.S. Feng, A.I. Aliagan, N. Tombo, D. Draeger, J.C. Bopassa, RIP3 translocation into mitochondria promotes Mitofilin Degradation to increase inflammation and kidney injury after Renal ischemia-reperfusion, Cells-Basel 11 (12) (2022).
[51] R. Baidya, J. Gautheron, D.H.G. Crawford, H.L. Wang, K.R. Bridle, Inhibition of MLKL Attenuates necroptotic cell death in a Murine cell model of Hepatic Ischaemia injury, J. Clin. Med. 10 (2) (2021).
[52] A. Linkermann, J.H. Bräsen, M. Darding, M.K. Jin, A.B. Sanz, J.O. Heller, F. De Zen, R. Weinlich, A. Ortiz, H. Walczak, J.M. Weinberg, D.R. Green, U. Kunzendorf, S. Krautwald, Two independent pathways of regulated necrosis mediate ischemia-reperfusion injury, Proc. Natl. Acad. Sci. USA 110 (29) (2013) 12024–12029.
[53] M. Luedde, M. Lutz, N. Carter, J. Sosna, C. Jacoby, M. Vucur, J. Gautheron, C. Roderburg, N. Borg, F. Reisinger, H.J. Hippe, A. Linkermann, M.J. Wolf, S. Rose-John, R. Lüllmann-Rauch, D. Adam, U. Flögel, M. Heikenwalder, T. Luedde, y N. Fre, RIP3, a kinase promoting necroptotic cell death, mediates adverse remodelling after myocardial infarction, Cardiovasc. Res. 103 (2) (2014) 206–216.
[54] H. Chen, Y. Fang, J. Wu, H. Chen, Z. Zou, X. Zhang, J. Shao, Y. Xu, RIPK3-MLKL-mediated necroinflammation contributes to AKI progression to CKD, Cell Death Dis. 9 (2018) 878.
[55] S.R. Mulay, J. Desai, S.V. Kumar, J.N. Eberhard, D. Thomasova, S. Romoli, M. Grigorescu, O.P. Kulkarni, B. Popper, V. Vielhauer, et al., Cytotoxicity of crystals involves RIPK3-MLKL-mediated necroptosis, Nat. Commun. 7 (2016), 10274.
[56] N. Vanlangenakker, B.T. Vanden, D.V. Krysko, N. Festjens, P. Vandenabeele, Molecular mechanisms and pathophysiology of necrotic cell death, Curr. Mol. Med. 8 (3) (2008) 207–220.
[57] M. Huang, Z.X. Li, J. Chen, L. Chen, Y.Y. Li, Extracts of Bauhinia championii alleviate acute Neuronal injury after ischemic reperfusion by Improving endoplasmic reticulum stress-mediated Neuronal apoptosis, Curr Med Sci 42 (3) (2022) 483–490.
[58] Y. Xu, X.D. Wu, W.J. Hu, D.J. Yu, Z.D. Shao, W.F. Li, et al., RIP3 facilitates necroptosis through CaMKII and AIF after intracerebral hemorrhage in mice, Neurosci. Lett. (2021) 749.
[59] M. Santra, X.S. Liu, S. Santra, J. Zhang, R.L. Zhang, Z.G. Zhang, et al., Ectopic expression of doublecortin protects adult rat progenitor cells and human glioma cells from severe oxygen and glucose deprivation, Neuroscience 142 (3) (2006) 739–752.
[60] M. Vassalle, C.I. Lin, Calcium overload and cardiac function, J. Biomed. Sci. 11 (5) (2004) 542–565.
[61] P. Xie, Z.K. Ren, J. Lv, Y.M. Hu, Z.Z. Guan, W.F. Yu, Berberine ameliorates oxygen-glucose deprivation/reperfusion-induced apoptosis by inhibiting endoplasmic reticulum stress and autophagy in PC12 cells, Curr Med Sci 40 (6) (2020) 1047–1056.
[62] W. Zhao, Y. Song, Q.Q. Wang, S. Han, X.X. Li, Y. Cui, et al., Cryptotanshinone induces necroptosis through Ca2+ release and ROS production in vitro and in vivo, Curr. Mol. Pharmacol. 15 (7) (2022) 1009–1023.

[63] M.A. Neginskaya, E.V. Pavlov, S.S. Sheu, Electrophysiological properties of the mitochondrial permeability transition pores: channel diversity and disease implication, Biochim. Biophys. Acta Bioenerg. 1862 (3) (2021), 148357.
[64] X. Zeng, Y.D. Zhang, R.Y. Ma, Y.J. Chen, X.M. Xiang, D.Y. Hou, et al., Activated Drp1 regulates p62-mediated autophagic flux and aggravates inflammation in cerebral ischemia-reperfusion via the ROS-RIP1/RIP3-exosome axis, Military Med Res 9 (1) (2022).
[65] K.J. Wang, X.Y. Meng, J.F. Chen, K.Y. Wang, C. Zhou, R. Yu, et al., Emodin induced necroptosis and inhibited Glycolysis in the Renal cancer cells by enhancing ROS, Oxid. Med. Cell. Longev. 2021 (2021), 8840590.